Soft Matter

PAPER

View Article Online
View Journal | View Issue



Cite this: *Soft Matter*, 2015, **11**, 7515

# Diffusive dynamics of nanoparticles in ultra-confined media†

Jack Deodato C. Jacob,[a] Kai He,[a] Scott T. Retterer,[b] Ramanan Krishnamoorti*[a] and Jacinta C. Conrad*[a]

Received 10th June 2015,
Accepted 9th August 2015

DOI: 10.1039/c5sm01437a

www.rsc.org/softmatter

Differential dynamic microscopy (DDM) was used to investigate the diffusive dynamics of nanoparticles of diameter 200–400 nm that were strongly confined in a periodic square array of cylindrical nanoposts. The minimum distance between posts was 1.3–5 times the diameter of the nanoparticles. The image structure functions obtained from the DDM analysis were isotropic and could be fit by a stretched exponential function. The relaxation time scaled diffusively across the range of wave vectors studied, and the corresponding scalar diffusivities decreased monotonically with increased confinement. The decrease in diffusivity could be described by models for hindered diffusion that accounted for steric restrictions and hydrodynamic interactions. The stretching exponent decreased linearly as the nanoparticles were increasingly confined by the posts. Together, these results are consistent with a picture in which strongly confined nanoparticles experience a heterogeneous spatial environment arising from hydrodynamics and volume exclusion on time scales comparable to cage escape, leading to multiple relaxation processes and Fickian but non-Gaussian diffusive dynamics.



## Introduction

Understanding the dynamics of nanoparticle dispersions in complex confined media is required to optimize the transport of nanoparticles in applications such as drug delivery,[1,2] enhanced oil recovery,[3,4] environmental remediation, and water treatment.[5,6] Natural porous media, viscoelastic matrices, and complex biological systems all exhibit heterogeneity in pore structure and surface chemistry.[7–11] Particles must therefore be specifically tailored for transport through targeted media, as their mobility in heterogeneous porous media is affected by their size[12] and surface properties:[13] for example, modifying non-zero valent metal nanoparticles used for ground water remediation can prevent particles from agglomerating and becoming trapped by the soil.[13] Improved fundamental understanding of the factors influencing particle transport will aid the design of nanoparticles for these applications.

As one example, the diffusion of submicron particles confined in porous media is hindered by crowding, by the presence of immobile barriers, and by hydrodynamic and steric interactions between particles and confining walls. Thus particle diffusion typically becomes slower in confinement. In our earlier study of the diffusion of modestly confined nanoparticles, in media with effective void fractions ranging from 0.76 to 0.99, the diffusive dynamics of the nanoparticles slowed with confinement and the distribution of displacements became increasingly non-Gaussian.[14] Similar slowing of Fickian diffusion coincident with non-Gaussian distributions of particle displacements has been observed in a variety of systems, including hard sphere colloidal dispersions,[15,16] polymers in an array of pillars,[17] nanoparticles in a porous polymer matrix,[18] and colloids in a matrix of entangled F-actin polymers.[19] The widespread occurrence of Fickian but non-Gaussian diffusion suggests a general physical origin of these dynamics.[20] Proposed origins of these dynamics and their signatures include heterogeneity in the microenvironment,[15,16] a crossover between distinct dynamical regimes,[16] or confinement-induced vitrification.[21] Additionally, statistical models such as the Lorentz gas[22–24] (a single tracer diffusing in an array of scatterers) can exhibit slowed and/or anomalous diffusion arising from the interplay of dynamics and geometry. In experimental systems, particles also experience different hydrodynamic interactions at different points in the environment even at macroscopically dilute conditions, and these differences become greater as particles become more crowded at higher particle concentrations[16,25] or when more strongly confined.[26–28] To identify the mechanisms that affect diffusion at different confinements requires studies in model media that access a broad range of particle confinements.

Microfabrication techniques offer the ability to design model porous media with tunable pore size, pore connectivity, and surface wettability.[17,18,29,30] Using one class of micromodels that simulate natural porous media, arrays of micro- and nanoscale posts in silicon and glass microchannels,[14,31,32] earlier experiments examined weak to moderate confinements. Elucidating

[a] *Department of Chemical and Biomolecular Engineering, University of Houston, Houston, TX 77204-4004, USA. E-mail: ramanan@uh.edu, jcconrad@uh.edu*
[b] *Center for Nanophase Materials Sciences and BioSciences Divisions, Oak Ridge National Laboratory, Oak Ridge, TN, 37934, USA*

† Electronic supplementary information (ESI) available. See DOI: 10.1039/c5sm01437a

the effects of strong confinement on nanoparticle transport, however, requires well-controlled media with typical pore or pore throat sizes of less than one micron. For example, media with low void fractions would be interesting as models for natural porous media with very small pore throats, such as oil-bearing sandstones and shales.[33]

In this paper, we investigate the dynamics of nanoparticles diffusing in dense arrays of nanoposts with void fractions ranging from 0.38–0.89. To access this regime of strong confinement, arrays of silicon nanoposts arranged on a square lattice with edge-to-edge spacings of 400–2000 nm were fabricated using a combination of lithography and chemical vapor deposition techniques. The diffusion of nanoparticles was quantified in submicron confinement in these arrays using differential dynamic microscopy (DDM). In even the strongest confinement nanoparticle diffusion was isotropic; the mobility could hence be characterized by an average diffusion coefficient and by a stretching exponent, which was related to the heterogeneity of the diffusive dynamics. The slowing of diffusion with increased confinement was in good agreement with that predicted by models for hindered diffusion[28,34,35] incorporating only steric restrictions and hydrodynamic drag. The stretching exponent decreased approximately linearly with increasing confinement. The success of hindered diffusion models in describing the diffusivity of the nanoparticles suggests that volume exclusion and hydrodynamic interactions in strong confinement likely generate spatial heterogeneity, although contributions from the crossover in dynamics expected as particles escape the pores defined by the nanoposts cannot be excluded. These physical processes lead to Fickian but non-Gaussian nanoparticle dynamics. These findings improve our understanding of the origins of non-Gaussian particle mobility in strongly confined porous media.

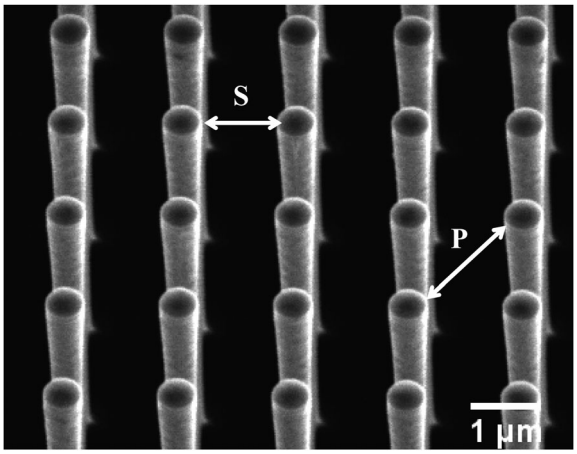


Fig. 1 Scanning electron micrograph of 500 nm-diameter cylindrical post arrays with 1.0 μm post spacing. *S* denotes the minimum spacing between posts and *P* denotes the diagonal spacing between posts of the square post array.

## Results and discussion

Time-resolved fluorescence optical micrographs were collected for nanoparticles of diameter 200, 300, and 400 nm diffusing in the bulk and in microfabricated post arrays (Fig. 1). The edge-to-edge spacing between posts ranged from 0.4 μm to 2 μm, corresponding to void fractions ($\theta$) of 0.38 to 1, throat confinement parameter ($\zeta$) of 0 to 0.76, and pore confinement parameters $\lambda$ of 0 to 0.39 (Table 1). From the time series of fluorescence images, the delay-time dependences of the azimuthally averaged image structure function $D(q, \Delta t)$ were calculated. To ensure that the dynamics were isotropic, azimuthal averaging in the $x$–$y$ plane was performed along arcs spanning $\pm 15^\circ$ in directions parallel to the sides and to the diagonals of the nanopost array. The dynamics of 300 nm particles diffusing freely and confined in different nanopost arrays are isotropic in all directions, as shown by comparing the image structure functions (ISFs) in Fig. 2. The ISFs measured along the open direction in the nanopost array ($90^\circ$) are indistinguishable from those measured along the diagonal of the post arrays ($135^\circ$) and from those obtained by averaging over all angles. The diffusive dynamics observed in this study remain isotropic across all confinements investigated and hence a single scalar diffusivity can be used to describe the dynamics within each nanopost array.

The image structure function (ISF) of particles freely diffusing in bulk can be fitted using a simple exponential model,

$$D(q, \Delta t) = A(q)\left[1 - \exp\left(-\frac{\Delta t}{\tau(q)}\right)\right] + B(q) \qquad (1)$$

where the signal prefactor $A(q)$ depends on the scattering properties of the particles, the light source and the system optics, $B(q)$ is the background noise of the system, and $\tau(q)$ is the $q$-dependent relaxation time.[36] In previous work on unconfined and freely-diffusing nanoparticles, we showed that the distribution of nanoparticle displacements was well described by a simple Gaussian function and that under these conditions the ISF was well fit by a simple exponential function.[37] Here eqn (2) describes the diffusion of unconfined particles in bulk (Fig. 3(a)). In previous work, we found that the prefactor $A(q)$ decreased monotonically with increasing $q$; for dilute samples ($\phi < 10^{-4}$) $B(q)$ depended only on the optics of the microscope and was independent of concentration and particle size.[37] Here $A(q)$ also decreases

Table 1 Post spacing, heights, void fraction, and confinement parameters for nanoparticles diffusing in post arrays

| Designed spacing [μm] | Measured spacing ($S$) [μm] | Height [μm] | Void fraction $\theta$ | | | $\zeta = d_{NP}/S$ | | | $\lambda = d_{NP}/P$ | | |
|---|---|---|---|---|---|---|---|---|---|---|---|
| | | | 200 nm | 300 nm | 400 nm | 200 nm | 300 nm | 400 nm | 200 nm | 300 nm | 400 nm |
| 2 | 1.93 ± 0.06 | 11.6 ± 0.1 | | | 0.89 | | | 0.22 | | | 0.13 |
| 1 | 1.08 ± 0.17 | 12.5 ± 0.1 | 0.85 | 0.80 | 0.75 | 0.19 | 0.28 | 0.37 | 0.11 | 0.17 | 0.23 |
| 0.8 | 0.84 ± 0.14 | 12.4 ± 0.1 | 0.79 | 0.72 | 0.65 | 0.24 | 0.36 | 0.48 | 0.14 | 0.22 | 0.29 |
| 0.4 | 0.40 ± 0.01 | 11.9 ± 0.1 | | 0.38 | | | 0.76 | | | 0.39 | |

 

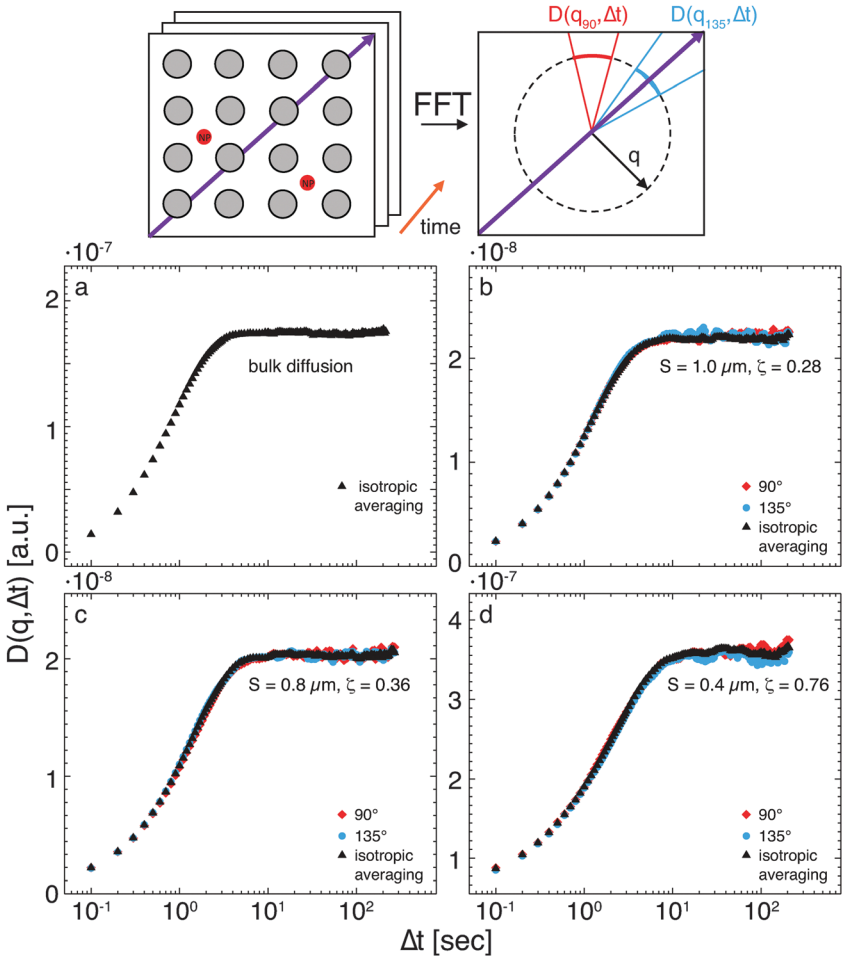


Fig. 2 (top) Schematic of experiments and averaging procedure. Azimuthal averaging is performed along arc lengths parallel to and perpendicular to the post arrays. (bottom) Image structure function $D(q, \Delta t)$ as a function of delay time $\Delta t$ at $q = 1\ \mu m^{-1}$ for 300 nm diameter particles (a) diffusing freely and in three different post arrays: (b) $S = 1.0\ \mu m$, $\zeta = 0.28$; (c) $S = 0.8\ \mu m$, $\zeta = 0.36$; (d) $S = 0.4\ \mu m$, $\zeta = 0.76$. Red diamonds represent particles travelling between posts, blue circles represent particles diffusing toward the posts, and black triangles represent the isotropic average of all particles.

monotonically. For this experimental setup, $B(q)$ is nearly constant across all wave vectors $q$ (Fig. S5–S7 in the ESI†). At high $q$ values, the short time plateaus of the ISFs are not well resolved. Therefore, to determine a best fit we choose as the initial value for $B(q)$ a wave-vector-independent value that was obtained from fitting of the low-$q$ ISF data.

When the nanoparticles are confined, the image structure function (ISF) can no longer be fitted using the simple exponential function in eqn (1). Neither the short-time plateau nor the turnover to the long-time plateau can be well described by an exponential, as shown in Fig. 3(b) and (c), and the deviation from an exponential fitting function becomes increasingly pronounced as confinement is increased. Instead, the ISF is fitted using a stretched exponential model,[14]

$$D(q, \Delta t) = A(q)\left[1 - \exp\left\{-\left(\frac{\Delta t}{\tau(q)}\right)^{r(q)}\right\}\right] + B(q) \qquad (2)$$

Four parameters ($A(q)$, $B(q)$, $\tau(q)$, and the stretching exponent $r(q)$) were extracted from the non-linear least squares fitting of the ISF data, as shown in Fig. 3 and in the ESI† in Fig. S5–S17. To interpret the diffusive dynamics we focus on two fitting parameters, $\tau(q)$ and $r(q)$.

The stretching exponent $r(q)$ measures the deviation of the distribution of particle displacements from Gaussian behavior. In previous work, we showed that the stretching exponent characterizing the non-Gaussian behavior of the distribution of particle displacements, obtained from particle-tracking, was proportional to the stretching exponent characterizing the deviation of the ISF from a simple exponential function, obtained by applying DDM to the same series of microscopy images.[14] The stretching exponents $r(q)$ obtained for all particles and all confinements in these experiments are shown as a function of wave vector $q$ in Fig. 4. We find that $r(q)$ is nearly constant at wave vectors below $q \approx 2\ \mu m^{-1}$. At higher wave vectors, $r(q)$ decreases slightly as $q$ increases; the value of $q$ at the crossover (*e.g.* for which $r(q) < 0.95\langle r(q)\rangle$) is approximately constant across the limited range of conditions for which we observe a decrease in $r(q)$ (reported in Table S1 of the ESI†). Given the magnitude of the error bars, especially at high $q$, no systematic understanding of the $q$-dependence of $r(q)$ is feasible.

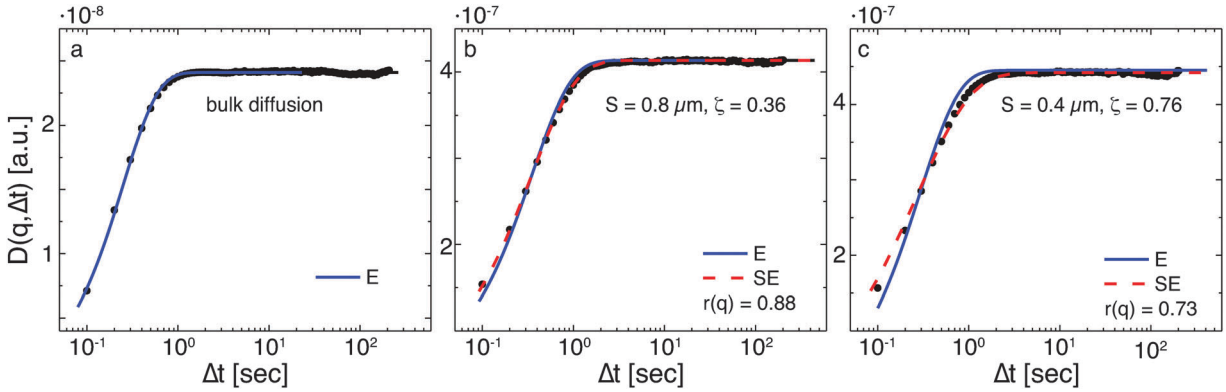


Fig. 3 Image structure function $D(q, \Delta t)$ as a function of delay time $\Delta t$ at $q = 1\ \mu m^{-1}$ for 300 nm diameter particles (a) diffusing freely and in two different post arrays: (b) $S = 0.8\ \mu m$, $\zeta = 0.36$; (c) and $S = 0.4\ \mu m$, $\zeta = 0.76$. Solid blue lines represent fits to a simple exponential model (E, eqn (1)) and dashed red lines represent fits to a stretched exponential model (SE, eqn (2)).

The relaxation time $\tau(q)$ is related to the diffusion coefficient $D$ *via* $D = 1/\tau(q)q^2$. Because the stretching exponent $r(q)$ varies somewhat across the wave vectors accessible in our setup, we first determine the sensitivity of the diffusivities to the parameters obtained from the fits to the ISF. The diffusivity is calculated from the wave-vector dependence of the relaxation time $\tau(q)$ *via* $D = 1/\tau(q)q^2$. To ascertain the robustness of the fitted diffusivities, we therefore compare $\tau(q)$ obtained using two different fit values for the stretching exponent: using the freely-fitted $r(q)$ values (shown in Fig. 4), and using the average value of $r(q)$, $\langle r(q)\rangle$, over the range of wave vectors ($0.5\ \mu m^{-1} < q < 2\ \mu m^{-1}$) for which $r$ is nearly independent of $q$. Both processes used to determine $r(q)$ produce values of $\tau(q)$ that are equal within the errors of the measurement, as shown in Fig. 5. We conclude that the relaxation time $\tau(q)$ is insensitive to the details of the fitting process and is robust for our measurements, and use $\langle r(q)\rangle$ to obtain $\tau(q)$ for each combination of particle size and nanopost spacings. In all experiments, $\tau(q)$ scales as $q^{-2}$ over the range of accessible $q$ values investigated (Fig. 6 and Fig. S18–S20 in the ESI†), indicating that the dynamics remain Fickian diffusive over these length and time scales. At a fixed value of $q$, the relaxation time $\tau(q)$ increases as the spacing between posts decreases, indicating that increasing confinement slows the diffusive dynamics of the nanoparticles.

We calculate $D$ for each combination of particle size and post spacing from the slope of $\tau(q)$ *versus* $q^2$. The resulting relative diffusivities $D/D_0$ decrease as void fraction $\theta$ is decreased and confinement parameters $\zeta$ and $\lambda$ are increased, as shown in Fig. 7, and fall onto a single curve for the three sizes of nanoparticles studied here. Initially, the decrease in relative diffusivity is nearly linear with $\theta$ and $\zeta$, as also reported in our earlier study;[14] particles experiencing the strongest confinements, however, exhibit diffusivities that are somewhat larger than those expected by extrapolating from low-to-moderate confinements. For the strongest confinement, where the minimum distance between posts is ~1.3 times the diameter of the nanoparticle, the particle diffusivity decreases to ~40% of that in the bulk. This decrease is similar in magnitude to that previously measured for nanoparticles diffusing very close to surfaces; for example, the diffusivity of a nanoparticle confined within a cylindrical cavity decreased from 75% to 45% of the bulk diffusivity when the distance between the particle and wall was reduced from nine to three particle diameters.[26]

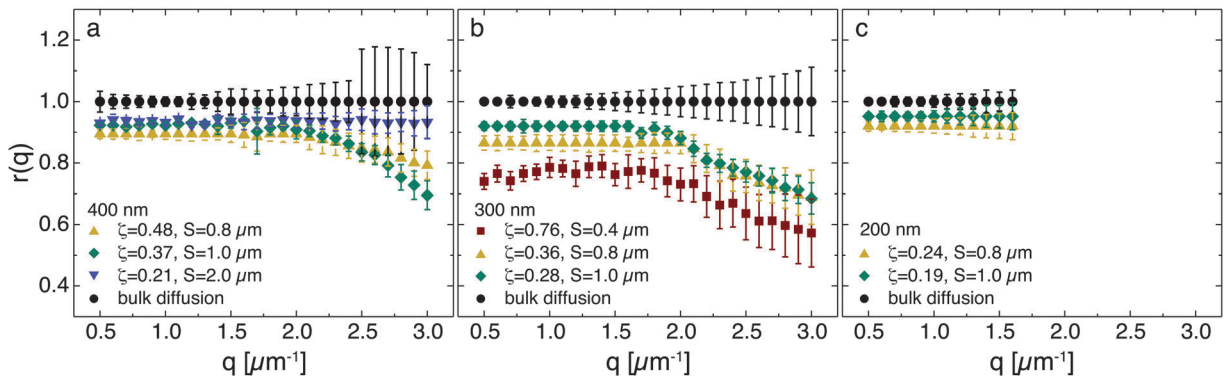


Fig. 4 Stretching exponent $r(q)$ as a function of the magnitude of the wave vector $q$ (in $\mu m^{-1}$) for (a) 400 nm nanoparticles diffusing in the bulk (black circles) and in post arrays with $S = 2\ \mu m$, $\zeta = 0.21$ (blue down triangles), $S = 1\ \mu m$, $\zeta = 0.37$ (green diamonds) and $S = 0.8\ \mu m$, $\zeta = 0.48$ (yellow up triangles); (b) 300 nm nanoparticles diffusing in the bulk (black circles) and in post arrays with $S = 1\ \mu m$, $\zeta = 0.28$ (green diamonds), $S = 0.8\ \mu m$, $\zeta = 0.36$ (yellow up triangles) and $S = 0.4\ \mu m$, $\zeta = 0.76$ (red squares); (c) 200 nm nanoparticles diffusing in the bulk (black circles) and in post arrays with $S = 1\ \mu m$, $\zeta = 0.19$ (green diamonds) and $S = 0.8\ \mu m$, $\zeta = 0.24$ (yellow up triangles).

 

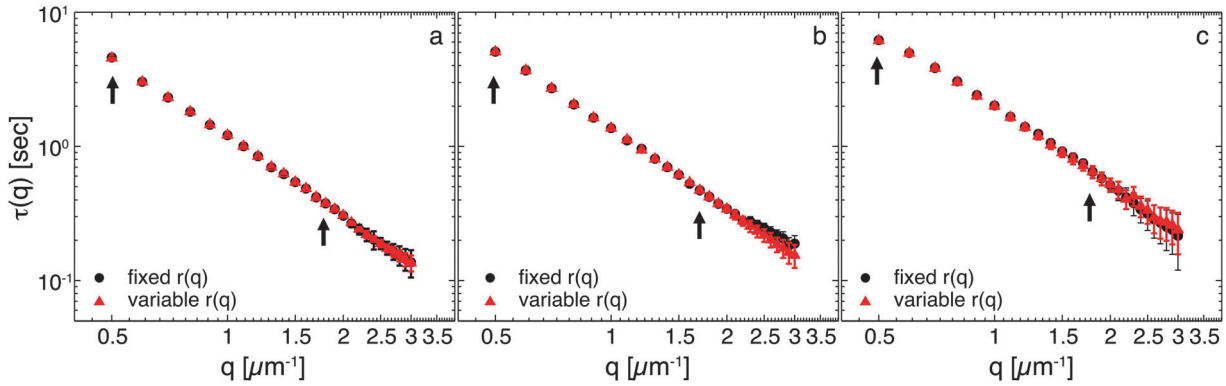


Fig. 5 Relaxation time $\tau(q)$ (in seconds) as a function of the magnitude of the wave vector $q$ (in $\mu m^{-1}$) for 300 nm nanoparticles diffusing in post arrays with (a) $S = 1\ \mu m$, with $r(q)$ fixed at $\langle r(q)\rangle = 0.92$ and $r(q)$ varied from $q = 0.63–0.92\ \mu m^{-1}$; (b) $S = 0.8\ \mu m$, with $r(q)$ fixed at $\langle r(q)\rangle = 0.89$ and $r(q)$ varied from $q = 0.74 – 0.89\ \mu m^{-1}$; and (c) $S = 0.4\ \mu m$, with $r(q)$ fixed at $\langle r(q)\rangle = 0.73$ and $r(q)$ varied from $q = 0.56–0.73\ \mu m^{-1}$. Black arrows indicate the range of wave vectors over which the average stretching exponent $\langle r(q)\rangle$ is calculated.

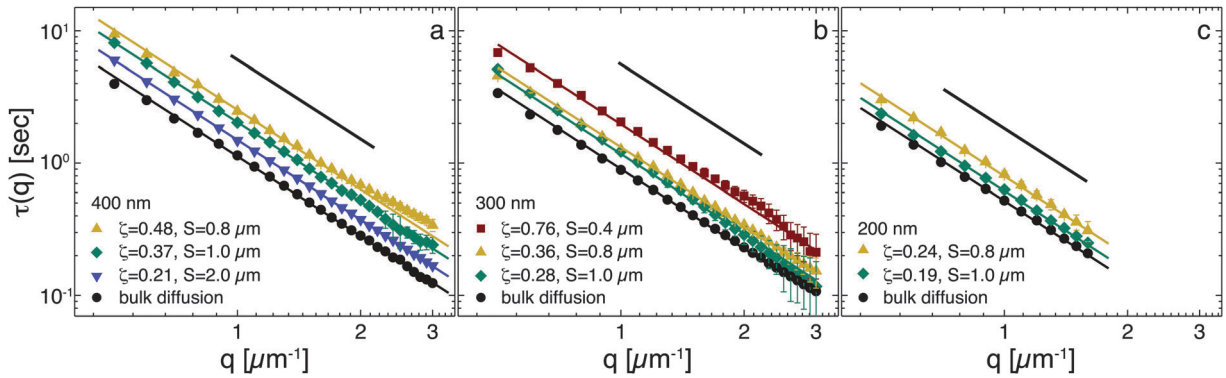


Fig. 6 Relaxation time $\tau(q)$ (in seconds) as a function of the magnitude of the wave vector $q$ (in $\mu m^{-1}$) for (a) 400 nm nanoparticles diffusing in the bulk (black circles) and in post arrays with $S = 2\ \mu m$, $\zeta = 0.21$ (blue down triangles), $S = 1\ \mu m$, $\zeta = 0.37$ (green diamonds), and $S = 0.8\ \mu m$, $\zeta = 0.48$ (yellow up triangles); (b) 300 nm nanoparticles diffusing in the bulk (black circles) and in post arrays with $S = 1\ \mu m$, $\zeta = 0.28$ (green diamonds), $S = 0.8\ \mu m$, $\zeta = 0.36$ (yellow up triangles), and $S = 0.4\ \mu m$, $\zeta = 0.76$ (red squares); (c) 200 nm nanoparticles diffusing in the bulk (black circles) and in post arrays with $S = 1\ \mu m$, $\zeta = 0.19$ (green diamonds) and $S = 0.8\ \mu m$, $\zeta = 0.24$ (yellow up triangles). Black lines indicate a function that decays as $q^{-2}$.

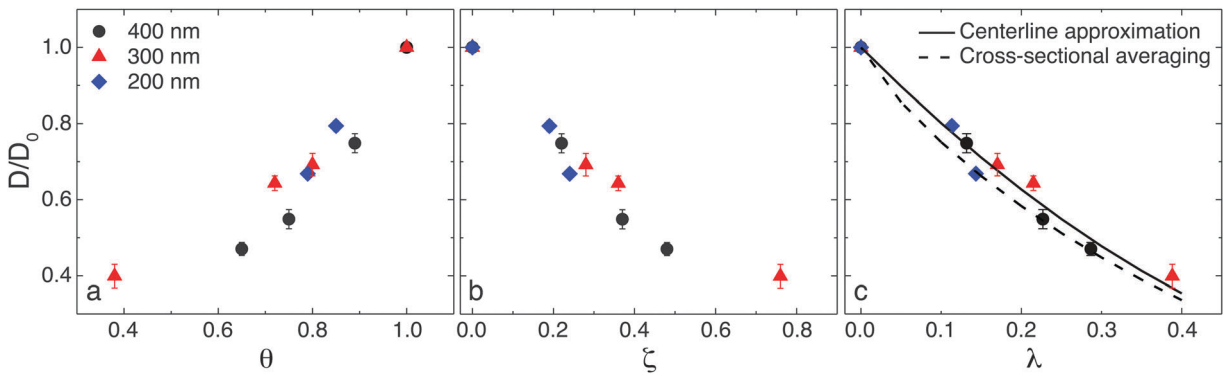


Fig. 7 Relative diffusivity $D/D_0$ as a function of (a) void fraction $\theta$ and confinement parameters (b) $\xi$ and (c) $\lambda$ for aqueous dispersions of nanoparticles of diameter of 400 nm (black circles), 300 nm (red triangles) and 200 nm (blue diamonds) measured by DDM. The solid and dashed black lines in (c) indicate the centerline approximation and the cross sectional averaging expressions for diffusion in slit pores (eqn (3) and (4)).

The slowing of nanoparticle diffusion observed here is reminiscent of that observed in a statistical model, the Lorentz gas.[23,24] In this family of models, diffusive-like motion of a single tracer particle arises from its interactions with an array of scatterers. We compare the slowing of the diffusion in our system to that obtained for two Lorentz gas systems, 2-d square[38] and hexagonal[39] lattices. In the long-time limit, our particles move diffusively (with diffusion scaling linearly with

time), whereas in the 2-d square lattice gas diffusion scales as $\sim t \log t$ [ref. 38]. In 2-d hexagonal lattices confinement is parameterized by the minimum spacing between scatterers, normalized by the post radius, $w = S/d_P$. To account for the finite size of the nanoparticles we define an effective confinement $w = (S - d_{NP}) \Big/ \left(\frac{d_P}{2} + \frac{d_{NP}}{2}\right)$. Studies of the diffusivity of Lorentz gases in 2-d hexagonal lattices focus on the high-density regime $\left(w < \frac{4}{\sqrt{3}} - 2 \approx 0.31\right)$. Our study accesses $0.25 < w < 3.56$ and includes only one data point in the high density regime: for $w \approx 0.25$, $D/D_0 \approx 0.40$. This value is somewhat larger than the value reported in computer simulations ($D/D_0 \approx 0.2$).[40]

To understand the origins of the reduced diffusivity, we consider several physical factors. The particles are stabilized with a nonionic surfactant and are negatively charged; the silica-coated posts are also negatively charged. We therefore expect that chemical interactions between the particles and posts are negligible: screened electrostatic interactions prevent particles from sticking to the posts and ensure that van der Waals interactions do not significantly affect diffusion. Instead, we posit that the decrease in relative diffusivity as nanoparticles become more confined arises from the interplay of hydrodynamic interactions and steric repulsion of the nanoparticles with the posts as the post density increases.[31,41,42] A particle diffusing in an unbounded fluid experiences a hydrodynamic drag force that opposes its direction of motion. Close to a solid surface, however, this drag force on the particle increases and hence particle diffusion becomes hindered.[4,43–45] Furthermore, hydrodynamic interactions become increasingly important as nanoparticles become more confined, due to the increased steric repulsion that particles experience when they approach hard walls.[46]

To test the idea that the decrease in diffusion results from hydrodynamic interactions and steric repulsion, we compare the relative diffusivities to predictions from analytical models for hindered diffusion valid for dilute dispersions. In this class of models, unstructured porous media are replaced by arrays of cylindrical[27,41] or slit pores[35] and the relative diffusivity of nanoparticles in these structured media is modeled by accounting for steric restriction and for particle-wall hydrodynamic interactions.[28] These models require several assumptions: (i) that the solvent (here, water) can be treated as a continuum; (ii) that the particle has adequate time to sample all cross-sectional positions in the pore; and (iii) that particle–particle interactions are negligible. Faxen derived the lag coefficients of a sphere between two parallel walls by approximating the drag on the sphere everywhere within the slit as equal to the drag on a particle sitting on the center line of the slit and obtained the centerline approximation[47]

$$\frac{D}{D_0} = (1-\lambda)\left(1 - 1.004\lambda + 0.418\lambda^3 + 0.21\lambda^4 - 0.169\lambda^5 + O\left(\lambda^6\right)\right) \quad (3)$$

valid for a relative solute size of $\lambda \leq 0.5$. Weinbaum *et al.* derived the lag coefficients of a sphere between two parallel walls[48] and averaged the results over the cross-section to calculate the relative diffusivities at different points between the plates.[49] Dechadilok *et al.* performed a least-squares fitting of these diffusivities and produced the cross-sectional averaging expression[28]

$$\frac{D}{D_0} = 1 + \frac{9}{16}\lambda \ln \lambda - 1.19358\lambda + 0.4285\lambda^3 + 0.3192\lambda^4 + 0.08428\lambda^5 \quad (4)$$

valid for $\lambda \leq 0.8$. We fit the relative diffusivities as a function of the confinement parameter that incorporates the characteristic pore radius, $\lambda$, using eqn (3) and (4), and find that the dependence on $\lambda$ is in good agreement with that predicted by the hindered diffusion models, even though our geometry is not quite that of a slit pore; within our experimental errors, we cannot distinguish between the two models. We conclude that steric restrictions and hydrodynamic drag can generate the observed decrease in relative diffusivity for nanoparticles diffusing in post arrays.

The $q^{-2}$ dependence of the relaxation time, $\tau(q)$, obtained from the ISF, indicates that the dynamics of confined nanoparticles remains diffusive. The diffusivities extracted from the ISFs, however, are derived from averaged measurements of relaxation times; the extent to which the distribution of relaxation times deviates from a Gaussian distribution can be measured by the value of the stretching exponent, $r(q)$, obtained from fitting the ISFs. The stretching exponent $r(q)$ for particles freely diffusing in the bulk is equal to unity, indicating that a single relaxation process is involved and thus the displacement distributions of the particles are Gaussian. In moderate to strong confinement, however, the ISFs of particles cannot be fit with a simple exponential expression, as expected for a relaxation process with a single timescale; instead, to properly describe these ISFs requires a stretched exponential model. In disordered systems, stretched exponential distributions of relaxation times have been ascribed to competing relaxation processes with distinct relaxation times.[14,50] A value of $r(q) < 1$ in this study hence suggests the existence of multiple relaxation processes. To investigate the effect of confinement on relaxation processes we therefore examine the stretching exponent, averaged over the range of low $q$ values for which $r(q)$ does not depend on $q$ (Fig. 4). The average stretching exponent $\langle r(q) \rangle$ decreases as the particles are increasingly confined, as shown in Fig. 8, indicating that the distribution of nanoparticle displacements becomes more non-Gaussian with increasing confinement.

In our earlier study of nanoparticle diffusion in moderately confined nanopost arrays, the probability distributions of particle displacements obtained using particle tracking could not be fitted using a Gaussian distribution model even though the particles exhibited diffusive dynamics at all accessible time scales. Instead, a model combining a Gaussian distribution (for short displacements) and a stretched Gaussian distribution (for long displacements) was required to fit the distributions of particle displacements.[14] Similar stretched Gaussian distributions are needed to fit the distributions of displacements for the 400 nm particles in these experiments (Fig. S21–S23 in the ESI†). Given the observation of non-Gaussian dynamics, the diffusive dynamics measured in these experiments likely do not access the fully asymptotic hydrodynamic limit. Non-Gaussian distributions of

 

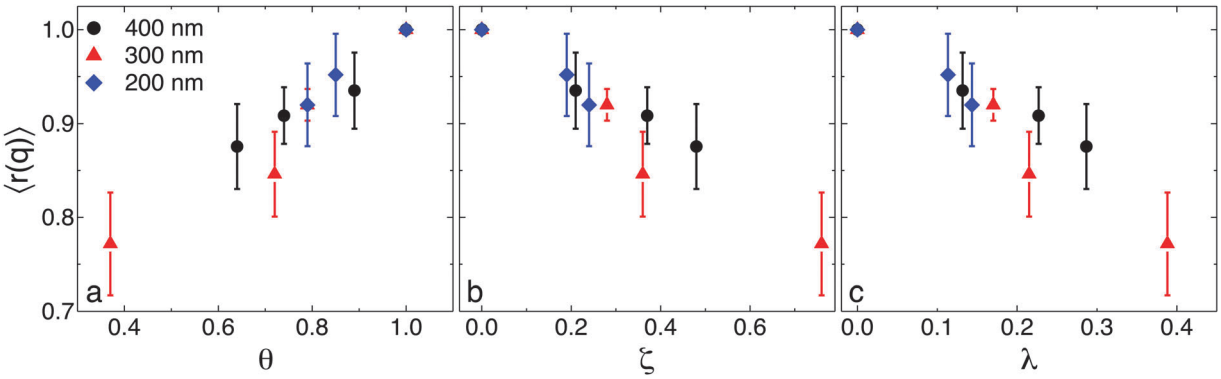


Fig. 8 Average stretching exponent $\langle r(q)\rangle$ as a function of (a) void fraction $\theta$ and confinement parameters (b) $\zeta$ and (c) $\lambda$ for aqueous dispersions of nanoparticles of diameter of 400 nm (black circles), 300 nm (red triangles), and 200 nm (blue diamonds) measured by DDM.

particle displacements reflect heterogeneity that is not averaged out on the time and length scales of the experiment.[15] Indeed, similarly Fickian but non-Gaussian Brownian diffusion has been reported in a wide range of systems[15,19,20,51,52] Although these varied results suggest that Fickian but non-Gaussian diffusion is a general feature of pre-asymptotic colloidal dynamics,[16] the physical origin of this phenomenon remains unclear and may arise from dispersity of either nanoparticle or microenvironment, vitrification due to caging-induced confinement,[21] and/or the existence of more than one diffusion process due to the heterogeneity of the system. In our experiments, polydispersity is an unlikely origin for the dynamics, as our nanoparticles are nearly monodisperse and we visually confirm that nanopost arrays are spatially uniform across the field of view in each experiment.

We next consider explanations related to spatial heterogeneity. Granick *et al.* suggested that the non-Gaussian distribution of particle displacements could be obtained by convolving independent Gaussian diffusion processes.[35] Our model nanopost arrays contain posts and void spaces and are thus spatially heterogeneous. At different locations within the system the nanoparticles experience different hydrodynamic interactions, which depend on the distance of the nanoparticles from the nanoposts. In support of this picture, our relative diffusivities are in good agreement with those predicted by hydrodynamic models (Fig. 7) that assume that the particles sample all cross-sectional positions within the pore volume. These results highlight the importance of hydrodynamics in diffusion of nanoparticles in confined media as it hinders the diffusion of the particles and affects the distribution of particle displacements.

Finally, we consider heterogeneous dynamics. Yethiraj *et al.* found that that Fickian but non-Gaussian dynamics arose in suspensions of particles of two different sizes.[16] On short time scales only the small tracer particles were mobile, whereas on long time scales both the small tracers and the large colloids were mobile. The dynamics of the small tracer particles were Fickian on short and on very long time scales, and the distributions of displacements were Gaussian in these limits. On intermediate time scales between these two limits, however, Yethiraj *et al.* found that diffusion remained Fickian but the displacement distribution of the tracers was non-Gaussian.[16] This result suggests that non-Gaussian distributions of dynamics may arise from the crossover between distinct dynamical regimes.

In our experiments, there are potentially two distinct diffusive processes. On short time scales particles are trapped within a pore defined by the posts; we expect that intrapore diffusion is affected by the pore size. On long time scales, however, particles can escape the pore and diffuse between the pores; we expect that interpore diffusion is affected by the pore throat size and the pore connectivity. The non-Gaussian dynamics observed in these experiments could arise during the crossover from intra-pore to inter-pore diffusion. To test this idea, we calculated the characteristic time scale on which particles escape from the pore interior, $\tau_e = \frac{\left[\frac{S+d_P}{2}\right]^2}{D}$. Our experiments span $\tau_e$, which ranges from 0.3–2.2 seconds (Table 2). Our experimental time scales thus can be classified as "intermediate," in accord with the idea that our measurements may not access fully asymptotic hydrodynamic limit of diffusion. Similarly, our measurements cannot conclusively determine whether our non-Gaussian dynamics arise from a crossover between dynamical regimes. As hydrodynamic interactions slow down the dynamics of the system and delay the onset of long-time behavior,[16] we cannot rule out a dynamical crossover solely on the basis of comparison to the hydrodynamic models. Across the range of accessible wave vectors, however, none of the ISFs obtained in confinement can be modeled using a single exponential function; the dynamics are always non-Gaussian.

Table 2 Characteristic escape time $\tau_e$ for each combination of particle size and post spacing investigated in this study

| Measured spacing between posts ($S$) [μm] | Particle diameter [μm] | Diffusion coefficient ($D$) [μm$^2$ s$^{-1}$] | $\tau_e = \frac{\left[\frac{S+d_P}{2}\right]^2}{D}$ [s] |
|---|---|---|---|
| 1.93 | 0.40 | 0.67 | 2.2 |
| 1.08 | 0.40 | 0.49 | 1.3 |
| 1.08 | 0.30 | 0.85 | 0.7 |
| 1.08 | 0.20 | 1.58 | 0.4 |
| 0.84 | 0.40 | 0.42 | 1.1 |
| 0.84 | 0.30 | 0.79 | 0.6 |
| 0.84 | 0.20 | 1.33 | 0.3 |
| 0.40 | 0.30 | 0.49 | 0.4 |

Our earlier study of nanoparticle diffusion in weak to moderate confinement, which combined DDM and particle tracking experiments,[14] also found that a stretched Gaussian model was required to describe the dynamics over all accessible time scales. As we cannot access either very short or very long time scales, however, it is possible that we are unable to detect the asymptotic hydrodynamic regimes of Fickian and Gaussian dynamics.[28,34]

# Conclusion

The dynamics of strongly confined nanoparticles diffusing in square nanopost arrays were investigated using differential dynamic microscopy. The relaxation times scaled diffusively across all wave vectors, and diffusion remained isotropic in all directions for even the most strongly confined nanoparticles. The decrease in diffusivity with increasing confinement could be described by models for hindered diffusion that accounted for steric restrictions and hydrodynamic interactions. The stretching exponent was less than one for all confined systems, consistent with non-Gaussian distributions of particle displacements, and decreased with increasing confinement. The decrease in the stretching exponent was consistent with the emergence of multiple relaxation processes for the dynamics. The distance between a particle and the nearest post varied at different locations within the post array, generating spatial heterogeneity in the hydrodynamic interactions. Given the success of hindered diffusion models in describing the particle diffusivity, the multiple relaxation processes likely reflected these spatial variations in hydrodynamic interactions, although contributions from the crossover in dynamics expected as particles escape the pores defined by the nanoposts could not be excluded. This study demonstrates that microfabricated silicon nanopost arrays can serve as models for natural porous media with small pore throats or pores. Moreover, these model systems can be engineered to exhibit some of the features of highly confined media by tuning the geometry and wettability of the posts. Studies identifying the dynamical features that result from such heterogeneity will generate additional insight into the processes affecting nanoparticle transport in natural porous media.

# Experimental methods

### Nanoparticle dispersions

Surfactant-stabilized Fluo-max dyed red aqueous fluorescent polystyrene particles with diameter ($d_{NP}$) of 400 nm were purchased from Thermo Fisher Scientific CDD. Dispersions were diluted with deuterium oxide (Sigma-Aldrich) to a volume fraction of $\varphi = 1 \times 10^{-5}$, corresponding to a number density of $2.8 \times 10^{8}$ ml$^{-1}$ for 400 nm nanoparticles, to minimize hydrodynamic interactions between the particles. A detailed description of these materials and the sample preparation protocol are provided in an earlier publication.[37]

### Fabrication and characterization of cylindrical nanopost arrays

Square silicon nanopost arrays of height $\sim$12 μm were fabricated in microfluidic chips to study the effect of extreme confinement on nanoparticle diffusion. Nanopost arrays with areas of 250 μm × 250 μm were uniformly arranged in a 2 mm × 0.8 mm microfluidic channel. The spacing between posts in each array was systematically varied from 0.4 to 2 μm (Fig. 1). Procedures for fabrication of the nanopost arrays are provided in an earlier publication.[14,31]

From the diameter and spacing of the posts, measured using scanning electron microscopy (SEM), we calculated three metrics to describe the confinement experienced by the nanoparticles (Table 1). The void fraction, $\theta$, was determined from:

$$\theta = \frac{(S + d_P)^2 - \frac{3}{4}(d_P + d_{NP})^2}{(S + d_P)^2} \quad (5)$$

where $S$ is the edge-to-edge spacing between posts, $d_P$ is the diameter of the silicon posts, and $d_{NP}$ is the diameter of the nanoparticles. Two additional confinement parameters describing the confinement experienced in different locations within the array were defined based on the separation between posts. The typical throat confinement, experienced by nanoparticles located between two posts, was $\zeta = d_{NP}/S$; the typical pore confinement, experienced by nanoparticles located in the center of the square lattice, was $\lambda = d_{NP}/P$, where $P$ is the diagonal distance between posts in the square array (Fig. 1). The characterization of the post arrays is summarized in Table 1.

### Experimental protocols

Silicon-based microchannels were sealed by a 4 mm thick layer of polydimethylsilane elastomer (PDMS, Sylgard 184, Dow Corning). Ports were punched in the PDMS using a Harris Uni-Core (Ted Pella, Inc., I.D. 0.75 mm) to allow fluid access to the microchannels. Oxygen plasma was used to oxidize the PDMS and microchannel surfaces and thereby promote a strong bond between the two surfaces. The ports on the PDMS were aligned with those of the microchannel to form a microfluidic device.[14]

Nanoparticle dispersions were injected into microchannels using a syringe pump (Harvard Apparatus, Pump 11 Pico Plus Elite). Tygon microbore tubing (i.d. 0.01″ and o.d. 0.03″, Cole Parmer, Vernon Hills, IL) was used to connect the PDMS port and 1 ml plastic syringes (Becton Dickinson, Franklin Lakes, NJ) with a stainless steel blunt needle (30 gauge Luer polypropylene hub, length 1/2″, Small Parts). After microchannels were filled with nanoparticle dispersions, the ports were closed to form a hermetic system. Nanoparticles diffusing in the sealed systems were imaged on an Olympus BX51 upright microscope equipped with a 50× objective (Olympus LMPlanFl N, numerical aperture of 0.5) using a Qiclick digital CCD camera (pixel size of 0.258 ± 0.002 μm per pixel, QIClick-F-M-12, Canada) controlled by StreamPix 5 software (Norpix, Canada). Reflected light was used to locate each rectangular post array on the microchannel, as the opacity of the silicon wafer prevented the use of transmitted light. The system was then switched to fluorescence mode to image the nanoparticle dispersions at the $z$ plane corresponding to the midpoint of the posts. In the microscopy experiments, we collected typically 5000 images over an area of 179.6 μm × 134.2 μm (corresponding to 696 pixels × 520 pixels) at a frame rate of

 

10 frames per second (fps) for 300 and 400 nm particles and 5 fps for 200 nm particles. Particles diffuse in quasi-two-dimensional confinement in the $x$–$y$ plane and remain in the field of view for the duration of the experiment. Occasional motion in or out of the plane of focus for a short time period breaks the trajectory, and thus we typically track particles for 100–1000 frames. Edge effects were precluded from our data collection and analysis as the field of view was smaller than the post array and care was taken to center the field of view with that of the array.

### Differential dynamic microscopy

We implemented a differential dynamic microscopy (DDM) algorithm and applied it to the fluorescence microscopy time series to analyze the diffusive dynamics of nanoparticle in strong confinement. Briefly, we subtracted pairs of images that were separated by a fixed lag time $\Delta t$, then calculated the Fourier spectrum of the intensity fluctuations in this time series of image differences to obtain the image structure function (ISF) $D(q, \Delta t)$. The ISF was fitted to different models to obtain the characteristic relaxation time $\tau(q)$. Detailed protocols for image processing and data analysis were described in previous papers[14,37,53] and are summarized in the ESI.† The one-dimensional DDM data were analyzed with non-linear least-squares fitting based on the Levenberg–Marquardt algorithm using Origin software (OriginLab, Northampton, MA). To validate the diffusivities extracted from DDM, we applied particle-tracking algorithms[54] to image series of 400 nm particles and directly calculated the diffusivities from the ensemble-averaged mean-square displacements of the particles. The diffusivities measured using DDM for the 400 nm nanoparticles were in excellent agreement with those obtained from the particle-tracking analysis, as also shown in our previous work.[14]

The accessible range of wave vectors $q$ is determined by the optical train of the microscopy setup.[37] The minimum accessible scattering wave vector $q_{min} = 2\pi/L$ is inversely proportional to the largest dimension of the image, $L$. $q_{max}$ is the smallest resolvable distance that a particle can travel between two successive images and is estimated as $(q_{max})^2$ = frame rate/$D_0$, where $D_0$ is the diffusivity of freely diffusing nanoparticles. The range of $q$ values was 0.5–3 $\mu m^{-1}$ for the 300 and 400 nm particles and 0.5–1.6 $\mu m^{-1}$ for the 200 nm particles.

## Acknowledgements

R.K. and K.H. acknowledge the support of the Gulf of Mexico Research Initiative (Consortium for Ocean Leadership Grant SA 12-05/GoMRI-002). J.C.C. acknowledges the support of the National Science Foundation (DMR-1151133) and the Welch Foundation (E-1869). A portion of this research was conducted at the Center for Nanophase Materials Sciences, which is sponsored at Oak Ridge National Laboratory by the Scientific User Facilities Division, Office of Basic Energy Sciences, U.S. Department of Energy.

## References

1 O. C. Farokhzad and R. Langer, *ACS Nano*, 2009, **3**, 16–20.
2 R. Tang, C. S. Kim, D. J. Solfiell, S. Rana, R. Mout, E. M. Velázquez-Delgado, A. Chompoosor, Y. Jeong, B. Yan, Z.-J. Zhu, C. Kim, J. A. Hardy and V. M. Rotello, *ACS Nano*, 2013, **7**, 6667–6673.
3 A. Roustaei, S. Saffarzadeh and M. Mohammadi, *Egypt. J. Pet.*, 2013, **22**, 427–433.
4 H. Zhang, A. Nikolov and D. Wasan, *Energy Fuels*, 2014, **28**, 3002–3009.
5 W.-x. Zhang, J. Cao and D. Elliott, *Nanotechnology and the Environment*, American Chemical Society, 2004, vol. 890, pp. 248–255.
6 C. M. Kocur, A. I. Chowdhury, N. Sakulchaicharoen, H. K. Boparai, K. P. Weber, P. Sharma, M. M. Krol, L. Austrins, C. Peace, B. E. Sleep and D. M. O'Carroll, *Environ. Sci. Technol.*, 2014, **48**, 2862–2869.
7 N. Fakhri, F. C. MacKintosh, B. Lounis, L. Cognet and M. Pasquali, *Science*, 2010, **330**, 1804–1807.
8 F. Amblard, A. C. Maggs, B. Yurke, A. N. Pargellis and S. Leibler, *Phys. Rev. Lett.*, 1996, **77**, 4470–4473.
9 D. L. Koch and J. F. Brady, *Phys. Fluids*, 1988, **31**, 965–973.
10 P. I. Hurtado, L. Berthier and W. Kob, *Phys. Rev. Lett.*, 2007, **98**, 135503.
11 F. Roosen-Runge, M. Hennig, F. J. Zhang, R. M. J. Jacobs, M. Sztucki, H. Schober, T. Seydel and F. Schreiber, *Proc. Natl. Acad. Sci. U. S. A.*, 2011, **108**, 11815–11820.
12 L. Shang, K. Nienhaus and G. Nienhaus, *J. Nanobiotechnol.*, 2014, **12**, 5.
13 B. Schrick, B. W. Hydutsky, J. L. Blough and T. E. Mallouk, *Chem. Mater.*, 2004, **16**, 2187–2193.
14 K. He, F. Babaye Khorasani, S. T. Retterer, D. K. Thomas, J. C. Conrad and R. Krishnamoorti, *ACS Nano*, 2013, **7**, 5122–5130.
15 J. Guan, B. Wang and S. Granick, *ACS Nano*, 2014, **8**, 3331–3336.
16 G. Kwon, B. J. Sung and A. Yethiraj, *J. Phys. Chem. B*, 2014, **118**, 8128–8134.
17 D. Wang, C. He, M. P. Stoykovich and D. K. Schwartz, *ACS Nano*, 2015, **9**, 1656–1664.
18 M. J. Skaug, L. Wang, Y. Ding and D. K. Schwartz, *ACS Nano*, 2015, **9**, 2148–2156.
19 B. Wang, S. M. Anthony, S. C. Bae and S. Granick, *Proc. Natl. Acad. Sci. U. S. A.*, 2009, **106**, 15160–15164.
20 B. Wang, J. Kuo, S. C. Bae and S. Granick, *Nat. Mater.*, 2012, **11**, 481–485.
21 M. Spanner, S. Schnyder, F. Höfling, T. Voigtmann and T. Franosch, *Soft Matter*, 2013, **9**, 1604–1611.
22 F. Höfling and T. Franosch, *Rep. Prog. Phys.*, 2013, **76**, 046602.
23 C. P. Dettmann, *Hard Ball Systems and the Lorentz Gas*, Springer Berlin Heidelberg, 2000, pp. 315–365.
24 C. P. Dettmann, *Commun. Theor. Phys.*, 2014, **62**, 521–540.
25 V. N. Michailidou, G. Petekidis, J. W. Swan and J. F. Brady, *Phys. Rev. Lett.*, 2009, **102**, 068302.
26 H. B. Eral, J. M. Oh, D. van den Ende, F. Mugele and M. H. G. Duits, *Langmuir*, 2010, **26**, 16722–16729.
27 M. G. Davidson and W. M. Deen, *Macromolecules*, 1988, **21**, 3474–3481.

28 P. Dechadilok and W. M. Deen, *Ind. Eng. Chem. Res.*, 2006, **45**, 6953–6959.
29 V. Berejnov, N. Djilali and D. Sinton, *Lab Chip*, 2008, **8**, 689.
30 F. J. Galindo-Rosales, L. Campo-Deaño, F. T. Pinho, E. van Bokhorst, P. J. Hamersma, M. S. N. Oliveira and M. A. Alves, *Microfluid. Nanofluid.*, 2011, **12**, 485–498.
31 C. K. Choi, J. D. Fowlkes, S. T. Retterer, P. Siuti, S. Iyer and M. J. Doktycz, *ACS Nano*, 2010, **4**, 3345–3355.
32 S. K. Bhatia and D. Nicholson, *Chem. Eng. Sci.*, 2011, **66**, 284–293.
33 P. H. Nelson, *AAPG Bull.*, 2009, **93**, 329–340.
34 H. Brenner and L. Gaydos, *J. Colloid Interface Sci.*, 1977, **58**, 312–356.
35 Y. Pawar and J. L. Anderson, *Ind. Eng. Chem. Res.*, 1993, **32**, 743–746.
36 R. Cerbino and V. Trappe, *Phys. Rev. Lett.*, 2008, **100**, 188102.
37 K. He, M. Spannuth, J. C. Conrad and R. Krishnamoorti, *Soft Matter*, 2012, **8**, 11933–11938.
38 J. P. Bouchaud and P. Le Doussal, *J. Stat. Phys.*, 1985, **41**, 225–248.
39 J. Machta and R. Zwanzig, *Phys. Rev. Lett.*, 1983, **50**, 1959–1962.
40 R. Klages and C. Dellago, *J. Stat. Phys.*, 2000, **101**, 145–159.
41 S. G. J. M. Kluijtmans, J. K. G. Dhont and A. P. Philipse, *Langmuir*, 1997, **13**, 4982–4987.
42 R. Raccis, A. Nikoubashman, M. Retsch, U. Jonas, K. Koynov, H.-J. Butt, C. N. Likos and G. Fytas, *ACS Nano*, 2011, **5**, 4607–4616.
43 S. L. Dettmer, S. Pagliara, K. Misiunas and U. F. Keyser, *Phys. Rev. E: Stat., Nonlinear, Soft Matter Phys.*, 2014, **89**, 062305.
44 B. Lin, J. Yu and S. A. Rice, *Phys. Rev. E: Stat. Phys., Plasmas, Fluids, Relat. Interdiscip. Top.*, 2000, **62**, 3909–3919.
45 P. Huang and K. S. Breuer, *Phys. Rev. E: Stat., Nonlinear, Soft Matter Phys.*, 2007, **76**, 046307.
46 H. Brenner, *Chem. Eng. Sci.*, 1961, **16**, 242–251.
47 J. Happel and H. Brenner, *Low Reynolds number hydrodynamics: with special applications to particulate media*, Springer Netherlands, 1st edn, 1983.
48 P. Ganatos, R. Pfeffer and S. Weinbaum, *J. Fluid Mech.*, 1980, **99**, 755–783.
49 S. Weinbaum, *Lectures on mathematics in the life sciences. Some mathematical questions in biology – neurobiology*, 1981, vol. 15, pp. 119–192.
50 A. Bunde, S. Havlin, J. Klafter, G. Graff and A. Shehter, *Philos. Mag. B*, 1998, **77**, 1323–1329.
51 A. G. Zilman and R. Granek, *Phys. Rev. Lett.*, 1996, **77**, 4788–4791.
52 D. E. Masri, G. Brambilla, M. Pierno, G. Petekidis, A. B. Schofield, L. Berthier and L. Cipelletti, *J. Stat. Mech.: Theory Exp.*, 2009, **2009**, P07015.
53 K. He, S. T. Retterer, B. R. Srijanto, J. C. Conrad and R. Krishnamoorti, *ACS Nano*, 2014, **8**, 4221–4227.
54 J. C. Crocker and D. G. Grier, *J. Colloid Interface Sci.*, 1996, **179**, 298–310.

 